Nanoscale

ROYAL SOCIETY OF CHEMISTRY

PAPER

Check for updates

Cite this: *Nanoscale*, 2020, **12**, 19178

Electric field tuned anisotropic to isotropic thermal transport transition in monolayer borophene without altering its atomic structure

Zhonghua Yang,†[a,b] Kunpeng Yuan, †[b,c] Jin Meng[a] and Ming Hu *[b]

Received 27th April 2020,
Accepted 14th August 2020

DOI: 10.1039/d0nr03273e

rsc.li/nanoscale

Thermal anisotropy/isotropy is one of the fundamental thermal transport properties of materials and plays a critical role in a wide range of practical applications. Manipulation of anisotropic to isotropic thermal transport or *vice versa* is in increasing demand. However, almost all the existing approaches for tuning anisotropy or isotropy focus on structure engineering or materials processing, which is time and cost consuming and irreversible, while little progress has been made with an intact, robust, and reversible method. Motivated by the inherent relationship between interatomic interaction mediated phonon transport and electronic charges, we comprehensively investigate the effect of external electric field on thermal transport in two-dimensional (2D) borophene by performing first-principles calculations along with the phonon Boltzmann transport equation. Under external electric field, the lattice thermal conductivity of borophene in both in-plane directions first increases significantly to peak values with the maximum augmentation factor of 2.82, and the intrinsic anisotropy (the ratio of thermal conductivity along two in-plane directions) is boosted to the highest value of 2.13. After that, thermal conductivities drop down steeply and anisotropy exhibits oscillating decay. With the electric field increasing to 0.4 V Å^{-1}, the thermal conductivity is dramatically suppressed to 1/40 of the original value at no electric field. More interestingly, the anisotropy of the thermal conductivity decreases to the minimum value of 1.25, showing almost isotropic thermal transport. Such abnormal anisotropic to isotropic thermal transport transition stems from the large enhancement and suppression of phonon lifetime at moderate and high strength of electric field, respectively, and acts as an amplifying or reducing factor to the thermal conductivity. We further explain the tunability of phonon lifetime of the dominant acoustic mode by an electron localization function. By comparing the electric field-modulated thermal conductivity of borophene with the dielectric constant, it is found that the screened potential resulting from the redistributed charge density leads to phonon renormalization and the modulation of phonon anharmonicity and anisotropy through electric field. Our study paves the way for robust tuning of anisotropy of phonon transport in materials by applying intact, robust, and reversible external electric field without altering their atomic structure and would have a significant impact on emerging applications, such as thermal management of nanoelectronics and thermoelectric energy conversion.

1 Introduction

Heat transfer is one of the main forms of energy transfer in nature. Efficient manipulation of thermal transport in materials is one of the most appealing fundamental thermal physical problems, with two representative but opposing aspects: on the one hand, increasing the thermal conductivity of a material to eliminate the heat accumulating performance of electronic equipment is essential to extend its life; on the other hand, reducing the thermal conductivity of the material is significant in the thermoelectricity and thermal insulation field. In order to expand the application of new materials more widely, tremendous amounts of research efforts have been dedicated over the past years to exploring robust ways to effectively modulate thermal transport. While almost all the existing approaches for tuning thermal conductivity focus on structure engineering or materials processing, the robust and

[a]*College of Architecture and Civil Engineering, Shenyang University of Technology, Shenyang, 110870, China*
[b]*Department of Mechanical Engineering, University of South Carolina, Columbia, SC 29201, USA. E-mail: hu@sc.edu*
[c]*Key Laboratory of Ocean Energy Utilization and Energy Conservation of Ministry of Education, School of Energy and Power Engineering, Dalian University of Technology, Dalian 116024, China*

† These authors contributed equally to this work.

reversible method by applying external electric field receives less attention.

Borophene is a close relative of graphene and has been predicted for more than 10 years. Experimentally, quasi-planar B_{35} and B_{36} clusters with hexagonal vacancies were observed earlier, and they are viewed as a potential basis for extended 2D boron sheets.[1] However, unlike the great success of carbon materials, boron materials have received relatively less attention due to the huge challenges in experimental implementation. Until December 2015, borophene was grown successfully on single crystal Ag (111) substrates under ultrahigh-vacuum conditions and since then it has been attracting tremendous research interest due to its extraordinary physical and chemical properties.[2] In particular, thermal transport in different phases of borophene has become an attractive topic.[3–7] The anisotropic thermal transport and moderate thermal conductivity make borophene promising in applications of transparent conductors and thermal management.[8] Zhou *et al.*[9,10] pointed out that all the high frequency phonons of borophene travel in one direction, resulting in their high thermal conductivity. The anomalous behavior is further explained by electron density distribution which indicates that the electron density of borophene is highly anisotropic. Similarly, molecular dynamics simulation was performed by Mortazavi *et al.* to illustrate that the anisotropy of the thermal conductivity of borophene is attributed to the differences in the density of states of low-frequency range, which correlate with lower group velocities and possibly shorten phonon lifetimes along the zigzag direction.[11] The stability of anisotropy in borophene nanoribbons depends on the large-scale localization of electrons along boron rows. All line-edge borophene nanoribbons undergo similar edge reconstructions to form extra π bonds to stabilize the electron deficient edge atoms.[12] Xiao *et al.* used borophene instead of an α′-boron sheet and the lattice thermal conductivity of borophene was gained by the first-principles calculation. The value was 14.34 W m^{-1} K^{-1} at room temperature along the armchair, which was substantially smaller than that of graphene.[13] Gao *et al.*[14] confirmed that electron–phonon coupling constants in the two compounds are larger than that in MgB_2. The superconducting transition temperatures were determined to be 18.7 K and 24.7 K through the McMillan–Allen–Dynes formula. Xiao *et al.*[15] further showed that the superconductivity of borophene can be significantly enhanced by strain and charge carrier doping. Tensile strain can increase the transition temperature to 27.4 K, while hole doping can notably increase the transition temperatures to 34.8 K. The superior mechanical flexibility of borophene along the $\vec{b}$ direction was investigated through valence charge density. It was found that the bonds of B_1–B_2 in the intermediate layer are weakened with an increase in the *b*-axis strain, which causes an out-of-plane negative Poisson's ratio.[16] Wang *et al.*[4] further explained that the pristine borophene has significant in-plane Young's moduli and Poisson's ratio anisotropy due to its strong and highly coordinated B–B bonds.

It is not difficult to find out from previous research results that the force–electricity–heat of borophene is inseparable from electrostatic interactions. Based on this premise, we propose an idea to apply an external electric field to affect the interatomic electrostatic interaction and finally alter the thermal conductivity. In this paper, we demonstrate that the thermal conductivity of borophene, particularly the anisotropy of thermal transport in two different directions, is very sensitive to a vertical external electric field. Fundamental insight into the electric field-modulated lattice thermal conductivity and the anisotropy of the in-plane thermal transport is gained by analyzing the phonon anharmonicity from the microscopic view of the phonon parameters and the electronic structure. Our study provides solid evidence for robustly modulating phonon transport in low-dimensional materials by applying external electric field, which is expected to have broad impact on lots of applications, such as thermal management of nanoelectronics and thermoelectrics.

2 Computational model and methods

All the calculations are based on density functional theory (DFT) as implemented in the Vienna *ab initio* simulation package (VASP).[17–19] The Perdew–Burke–Ernzerhof (PBE)[20] functional of the generalized gradient approximation (GGA) is chosen as the exchange–correlation functional. The kinetic energy cutoff of the wave functions is set as 450 eV, and a Monkhorst–Pack[21] *k*-mesh of 27 × 15 × 1 is used to sample the Brillouin Zone (BZ). The lattice constants and internal coordinates are optimized until the atomic forces become less than 10^{-4} eV $Å^{-1}$. A large vacuum spacing of 20 Å is employed along the out-of-plane direction to eliminate the interaction between periodic images. To simulate a perpendicular electric field, VASP introduces dipole sheets in the middle of the vacuum regions, the electric field along the out-of-plane direction is applied and the dipole corrections are considered.[22]

It is well-known that the thermal conductivity is governed by the specific heat capacity, group velocity, and phonon lifetime:

$$\kappa_\alpha = \sum_\lambda c_{\mathrm{ph},\lambda} \nu_{\alpha,\lambda}^2 \tau_\lambda \tag{1}$$

where κ_α denotes the lattice thermal conductivity in the α direction, λ represents the phonon mode with wave vector **q** and phonon branch **s**, $\nu_{\alpha,\lambda}$ is the phonon group velocity of mode λ along the α direction, τ_λ is the phonon lifetime of mode λ, and c_{ph} refers to the phonon volumetric specific heat of each mode

$$c_{\mathrm{ph}} = \frac{k_\mathrm{B}}{NV} \frac{(\hbar\omega_\lambda/k_\mathrm{B}T^2)e^{\hbar\omega_\lambda/k_\mathrm{B}T}}{(e^{\hbar\omega_\lambda/k_\mathrm{B}T}-1)^2} \tag{2}$$

where k_B is the Boltzmann constant, N is the **q** points number in the first Brillouin zone, V is the unit cell volume, $\hbar$ is the reduced Planck constant, T is the absolute temperature, and ω is the phonon angular frequency of mode λ. The group velocity of phonon mode λ is the gradient of frequency concerning reciprocal space coordinates:

$$\nu_\lambda = \nabla_q \omega_\lambda. \quad (3)$$

The phonon lifetime is one of the key input parameters determining the lattice thermal conductivity. The finite lifetime of a specific phonon mode depends on various scattering mechanisms, such as the intrinsic phonon–phonon scattering, the phonon–isotope scattering, and the phonon–boundary scattering. The total phonon lifetime is expressed by Matthiessen's rule as:

$$\frac{1}{\tau_\lambda} = \frac{1}{\tau_\lambda^{anh}} + \frac{1}{\tau_\lambda^{\mathrm{iso}}} + \frac{1}{\tau_\lambda^{B}} \quad (4)$$

where τ_λ^{anh}, $\tau_\lambda^{\mathrm{iso}}$, and τ_λ^{B} are the intrinsic phonon–phonon scattering rates, the phonon–isotope scattering rates, and the phonon–boundary scattering rates, respectively.

Specifically, the lattice thermal conductivity (κ_l) is obtained by iteratively solving the linearized Boltzmann–Peierls transport equation as implemented in the ShengBTE package[23] which requires the inputs of second-order harmonic and third-order anharmonic interatomic force constants (IFCs). A 7 × 5×1 supercell and a Γ-centered 7 × 5×1 k-mesh are chosen to calculate the harmonic and anharmonic IFCs. The second-order harmonic IFCs are used to determine the phonon frequency and phonon eigenvector using the Phonopy code.[24] A script of thirdorder.py is used to obtain the third-order IFCs which can be evaluated based on the third-order derivatives of the total energy with respect to the atomic displacements. This program predicts the material's k_l without any other adjustable parameters except for the basic information of the chemical structure.

3 Simulation results and discussion

3.1 Electric field modulated geometry structure and system energy

The optimized structure of borophene is illustrated in Fig. 1 which shows the typical monolayer structure. Both optimized lattice constants a = 2.871 Å and b = 1.617 Å are consistent with previous theoretical calculations.[25] In this structure, the shortest B–B bond length is 1.617 Å, which is 0.251 Å shorter than the longest length, indicating that the strength of the B–B chemical bond is different along different directions. Two planes of a rectangular lattice form a buckled structure, with a buckling distance of 0.88 Å. By adding the diameter of the boron atom of 1.81 Å, the thickness of borophene is chosen as 2.69 Å. The electric field is applied along the downward (out-of-plane) direction as indicated by the arrow in Fig. 1(b).

The lattice constant and buckling distance change with the strength of the external electric field, as shown in Fig. 2. It can be seen in Fig. 2(a) that, as the electric field increases, the dipole moment increases linearly. In Fig. 2(b), both the lattice constant and buckling distance do not have noticeable change until the strength of the external electric field exceeds 0.04 V Å^{-1}. After that, all structural parameters increase in an exponential form with electric field and the buckling distance increases even faster. At an electric field of 0.2 V Å^{-1}, the

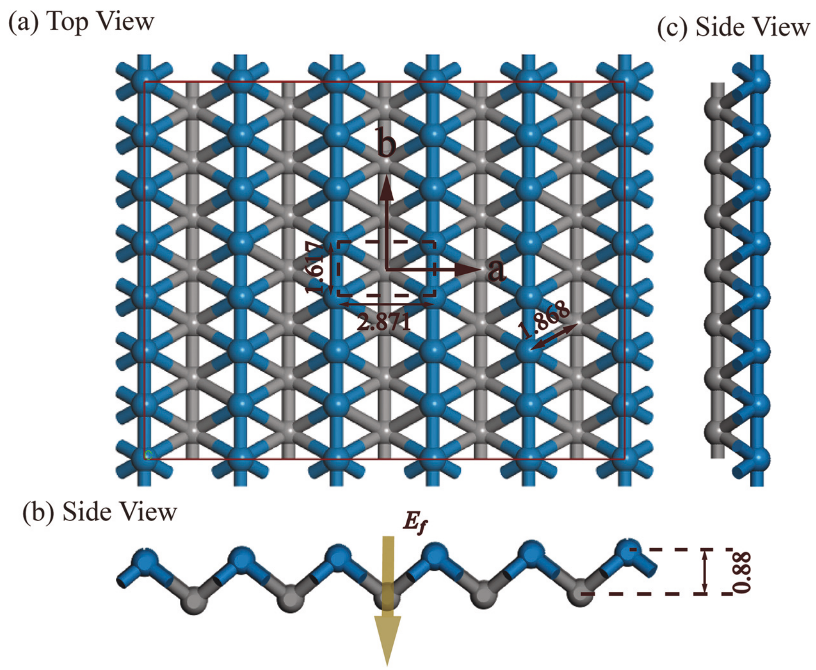

Fig. 1 The atomic structure of borophene in (a) top and (b) side views. The two in-plane directions ($\vec{a}$ and $\vec{b}$) are defined in the top panel. Atoms in different planes are distinguished by different colors (blue and gray) with a buckling distance of 0.88 Å. The primitive cells are shown by dashed lines. The electric field is applied along the downward out-of-plane direction as indicated by the arrow in the bottom panel.

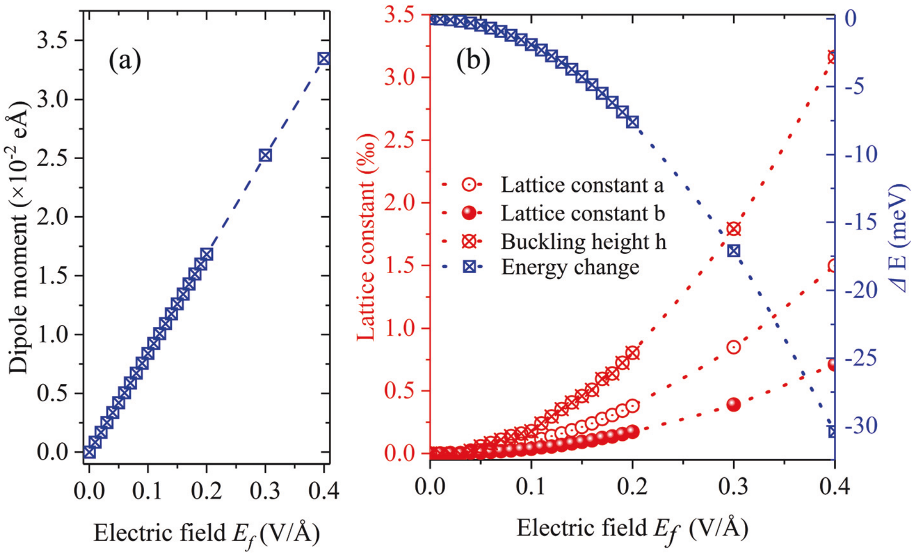

Fig. 2 (a) The dipole moment and (b) the changes in the atomic structure (left axis) and energy (right axis) as a function of the strength of external electric field.

lattice constant and buckling distance are only increased by 0.34‰ and 0.72‰, respectively. Thus, the buckled structure of borophene still remains stable. Furthermore, with the strength of the electric field increasing, the total energy of the borophene supercell decreases, showing a more thermodynamically stable structure in the external electric field, which is the basis for further phonon transport calculations.

3.2 Electric field tuned lattice thermal conductivity and anisotropy of thermal transport

Under the condition of considering the phonon–phonon scattering as determined by phonon anharmonicity, the lattice thermal conductivity (κ_l) of borophene is obtained by solving the phonon BTE. The thermal conductivity convergence of borophene with respect to the cutoff radius and Q-grid are fully examined as shown in Fig. 3. The convergence of the cutoff radius of anharmonic IFCs should be tested firstly, because the cutoff radius can be directly determined to get satisfactory thermal conductivity results based on the analysis of harmonic IFCs.[26] In order to quantify the strength of interatomic interactions which are described by harmonic IFCs, we calculated the normalized trace of interatomic force constant tensors.[27] According to this parameter, one can directly determine how large the cutoff radius should be to evaluate the anharmonic IFCs by effectively including the possibly strong interaction strength as revealed by the large trace value. Fig. 3(a) shows the normalized trace of IFCs in borophene, and it is clear that there exist strong interactions between boron atoms when the cutoff radius is less than 0.4 nm (seventh-nearest neighbors). When the threshold of the cutoff radius is bigger than 0.4 nm, the trace values are very weak, indicating negligible force constants. Similar conclusions can also be obtained by the convergence test of borophene thermal conductivity as shown in Fig. 3(b). Before the cutoff radius achieving the threshold of 0.4 nm, the borophene thermal conductivities along $\vec{a}$ and $\vec{b}$ directions drop dramatically, and the thermal conductivity converges quickly up to the seventh-nearest neighbors, which confirm the evaluation from the strength of the harmonic IFCs as shown in Fig. 3(a). It is also shown in Fig. 3(c) that the thermal conductivity of borophene possesses a well-converged behavior when the Q-grid is greater than 33 × 59 × 1. Therefore, considering both computational cost and accuracy, the interactions are truncated up to the seventh-nearest neighbors and the Q-grid is set as 33 × 59 × 1 for the following anharmonic IFC calculations.

Based on the converge test of anharmonic IFCs, the temperature dependent lattice thermal conductivity of borophene is shown in Fig. 4(a). The thermal conductivity of borophene with no electric field is remarkably anisotropic and unexpectedly low. Within the considered temperature range, for both in-plane directions [see definition in Fig. 1], the thermal conductivities of borophene decrease with increasing temperature. At room temperature, the thermal conductivities of borophene along $\vec{a}$ and $\vec{b}$ directions are 39.61 W m^{-1} K^{-1} and 73.48 W m^{-1} K^{-1}, respectively, which are significantly lower than that of graphene.[26] The thermal conductivity along the $\vec{b}$ direction is around 1.85 times that along the $\vec{a}$ direction. These results agree very well with the previous study.[28] Furthermore, the cumulative thermal conductivity with respect to the phonon mean free path (Λ) at 300 K is plotted as shown in Fig. 4(b), which is helpful for the study of the size effect on the ballistic or diffusive phonon transport. The cumulative thermal conductivities of borophene along $\vec{a}$ and $\vec{b}$ directions keep increasing as Λ increases, and then approach a plateau after Λ reaches 100 nm. It means that Λ is critical to affect the thermal conductivity of borophene when the nanostructure size is below the characteristic size.[29] To better understand the reason for anisotropic thermal conductivity, we compare the phonon

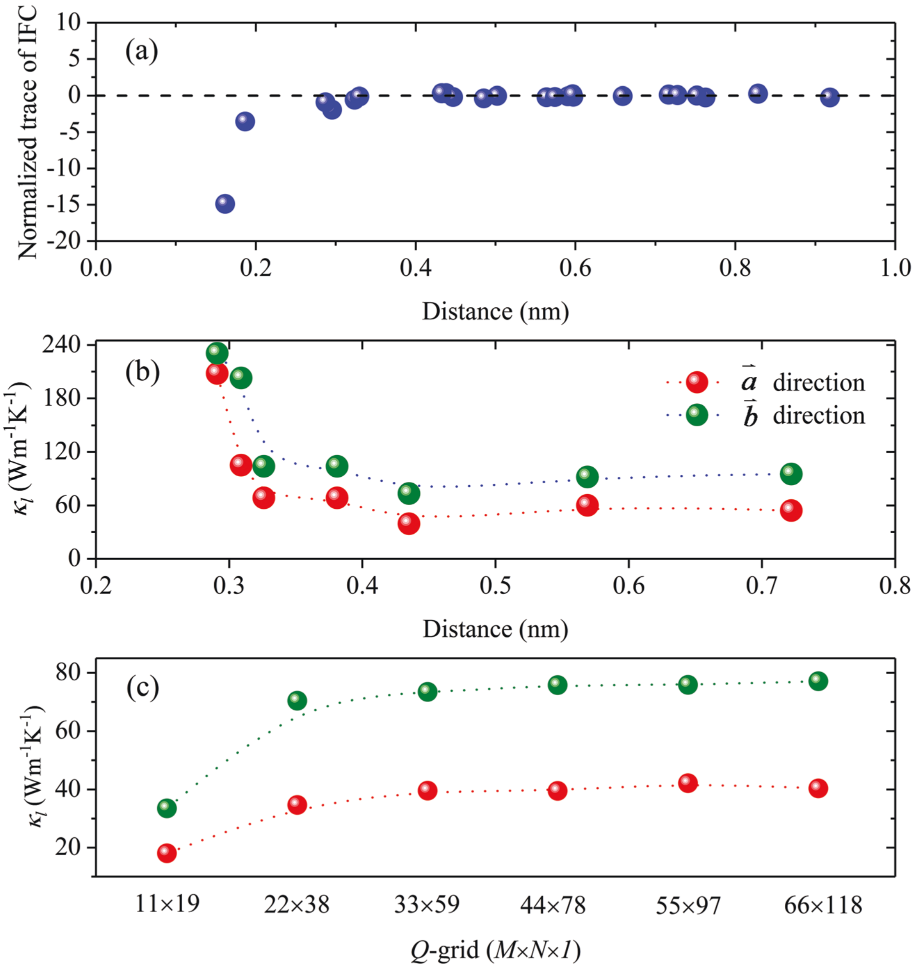

Fig. 3 (a) Normalized trace of interatomic force constant tensors *versus* atomic distances. (b) Convergence test of thermal conductivity with respect to cutoff radius. (c) Convergence test of thermal conductivity with respect to the *Q*-grid.

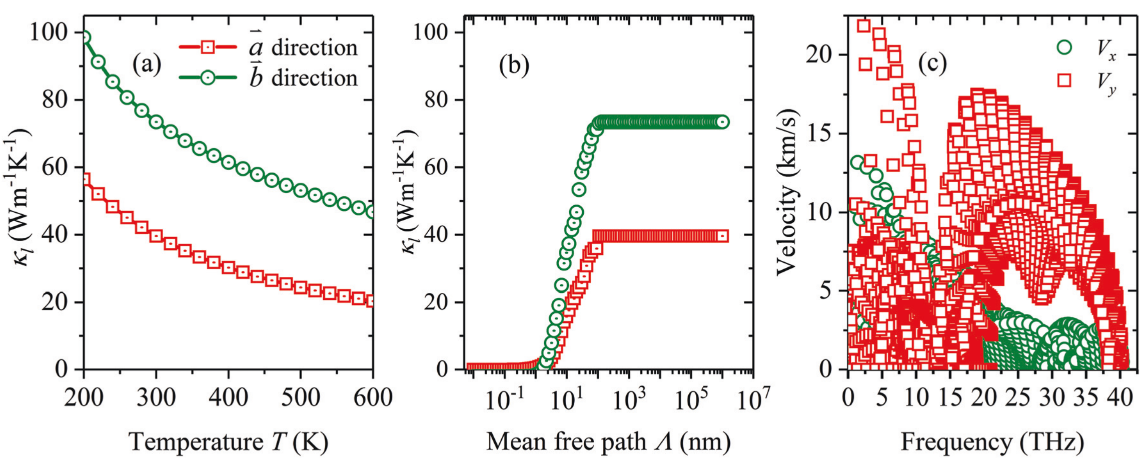

Fig. 4 (a) The temperature dependent lattice thermal conductivity along the *a*- and *b*-axis. (b) The mean free path dependent cumulative lattice thermal conductivity along the *a*- and *b*-axis. (c) Comparison of frequency dependent phonon group velocities in the two in-plane directions ($\vec{a}$ and $\vec{b}$).

group velocity of borophene along the two in-plane directions [Fig. 4(c)]. The maximum value of group velocity is 21.845 km s^{-1} which is similar to that of previous research results[28] (21.8 km s^{-1}) and that of graphene (21.9 km s^{-1}). Moreover, it is clearly seen that generally the phonon group velocities along the $\vec{b}$ direction are remarkably higher than those along the $\vec{a}$ direction, which is primarily responsible for the anisotropic thermal conductivity as found in Fig. 4(a).

Next, when the external electric field is switched on, the thermal conductivities of borophene along $\vec{a}$ and $\vec{b}$ directions first increase until the electric field reaches 0.04 V $Å^{-1}$ and then drops down steeply until the electric field reaches 0.4 V $Å^{-1}$ [see Fig. 5(a)]. However, the increase and decrease rates of thermal conductivity along $\vec{a}$ and $\vec{b}$ directions are different, which leads to a tremendous change in the anisotropy of the thermal transport in these directions, as we will discuss below. The maximum thermal conductivity values of borophene are 97.41 W m^{-1} K^{-1} and 207.25 W m^{-1} K^{-1} along $\vec{a}$ and $\vec{b}$ directions, respectively. The peak values at the electric field of 0.04 V $Å^{-1}$ are 2.46 and 2.82 times that of the thermal conductivities without external electric field, respectively. The lowest thermal conductivity values of borophene at the largest electric field of 0.4 V $Å^{-1}$ are 1.48 W m^{-1} K^{-1} and 1.85 W m^{-1} K^{-1} along $\vec{a}$ and $\vec{b}$ directions, respectively, which are only 3.74% and 2.52% of their respective thermal conductivities without external electric field. These results indicate that the external electric field can robustly modulate the phonon transport in 2D borophene. A quick evaluation of frequency resolved thermal conductivity as presented in Fig. 5(b) implies that the phonon transport in monolayer borophene with or without external electric field is always dominated by the phonon modes with frequency in the range of 7.5–10 THz, which is exactly the region of acoustic phonons [see Fig. 7 below]. In this frequency range, the phonon contribution to overall heat conduction in borophene is 53%, 78%, and 50% for an electric field of 0 V $Å^{-1}$, 0.04 V $Å^{-1}$, and 0.2 V $Å^{-1}$, respectively. This result is important for our further discussion and analysis below.

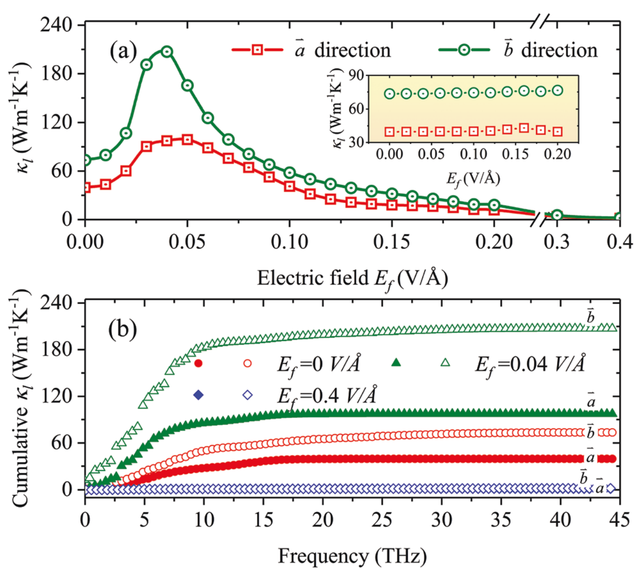

Fig. 5 (a) Lattice thermal conductivity of borophene at 300 K with different strengths of external electric field. (Inset) The effect of the atomic structure on lattice thermal conductivity. The abscissa represents the atomic structure of different electric fields (0–0.2 V $Å^{-1}$). (b) The frequency dependent cumulative thermal conductivity of borophene at 300 K with different strengths of external electric field.

More interestingly, the anisotropy of thermal conductivity of monolayer borophene can be dramatically tuned with different strengths of external electric field [see Fig. 6]. At an electric field of 0.04 V $Å^{-1}$, the ratio of thermal conductivity along the $\vec{b}$ direction to that along the $\vec{a}$ direction increases from 1.86 to 2.13 (by 15%). As the strength of the electric field increases further, the anisotropy of thermal conductivity of monolayer borophene exhibits an oscillating behavior. The lowest ratio of thermal conductivity along the $\vec{b}$ direction to that along the $\vec{a}$ direction reaches 1.25 at an electric field of 0.4 V $Å^{-1}$.

Before we analyze the detailed mechanism of the strong dependence of anisotropy on thermal transport in borophene, we first need to exclude an intuitive factor of the small structure change [see Fig. 2(b)], *i.e.* whether the thermal conductivity change is induced by the tiny atomic structure change or by the external electric field. To answer this question, herein we perform a computer experiment. We use the same optimized atomic structure under each different electric field and re-calculate the second-order harmonic and third-order anharmonic interatomic force constants without switching on the electric field and finally re-calculate the thermal conductivity. In this way, the obtained thermal conductivity is solely based on the effect of electric field, not on the effect of structure change. From the inset of Fig. 5(a), there is little variation in

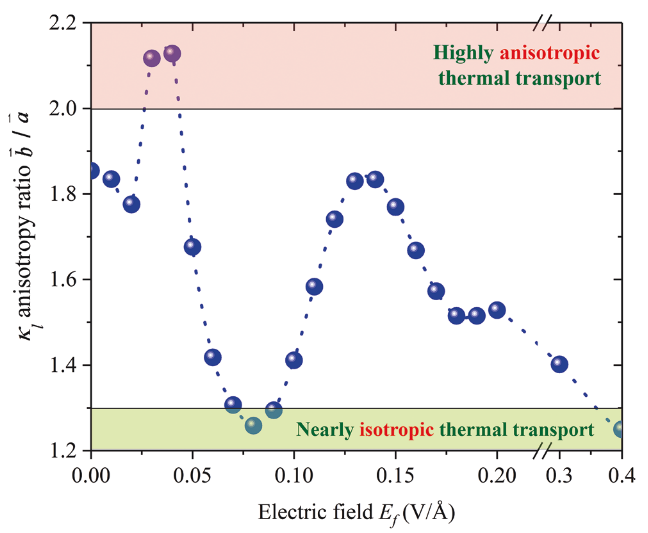

Fig. 6 Anisotropy ratio of borophene at room temperature as a function of the strength of external electric field. The upper and lower shaded area denotes the highly anisotropic and nearly isotropic thermal transport, respectively.

the thermal conductivity, which directly proves that the external electric field is indeed critical for the strong dependence of anisotropy on thermal transport in borophene as identified in Fig. 6.

3.3 Phonon dispersion of monolayer borophene

Phonon dispersion is crucial for the calculation of phonon transport properties. By using the finite displacement difference (FDD) method, we obtained the IFCs and hence the phonon dispersion relationship of borophene [see Fig. 7]. The high symmetry path of monolayer borophene is Γ–X–S–Y–Γ. The unit cell of borophene contains two atoms, resulting in six dispersion branches. The longitudinal acoustic (LA) and transverse acoustic (TA) branches correspond to vibration within the plane, and the other one (ZA) corresponds to out of plane vibration. Mainly attributed to the intrinsic buckled structure, three-acoustic branches of borophene present linear dispersion *versus* the wave vector around the Γ point, which is similar to silicene and phosphorene.[30,31] However, this behavior is different from that of the ZA branch of graphene, which has a quadratic dispersion around the Γ point.[32] It is worth mentioning that the ZA branch of borophene has a small imaginary frequency near the Γ point, which indicates that the lattice may exhibit instability.[2] However, the structure may be stable when supported by a suitable substrate, and such a small imaginary frequency should not significantly affect the thermal conductivity calculations, the same as reported in a previous study.[9] The average acoustic Debye temperature can be derived from:[33]

$$\frac{1}{\theta_{\mathrm{D}}^{1}} = \frac{1}{3}\left(\frac{1}{\theta_{\mathrm{ZA}}^{3}} + \frac{1}{\theta_{\mathrm{TA}}^{3}} + \frac{1}{\theta_{\mathrm{LA}}^{3}}\right) \tag{5}$$

where θ_i is obtained by $\theta_i = \hbar\omega_{i,\max}/k_{\mathrm{B}}$, and i is each acoustic branch (ZA, TA, and LA). $\omega_{i,\max}$ is the maximum of each phonon frequency at the zone boundary. The calculated average acoustic Debye temperature for borophene is 648 K, which is higher than that of monolayer MoS_2 (262.3 K)[31] and black phosphorene (500 K),[34] but lower than that of graphene (2300 K).[35] The higher Debye temperature indicates that borophene possesses a strong interatomic bonding.

On comparing phonon dispersions under different electric fields, we found that the phonon dispersions of borophene change very slightly. According to eqn (3), the phonon group velocity is given by the slope of the dispersion relationship. Due to the consistency of the phonon dispersion, the group velocity has no big change with different electric fields. However, the phonon dispersions of the acoustic modes along the $\vec{a}$ direction are generally much flatter than those along the $\vec{b}$ direction. Such a phenomenon implies that the phonon group velocity in the $\vec{a}$ direction is smaller than that in the $\vec{b}$ direction, which is the result shown in Fig. 4(c).

As previously analyzed, due to the anisotropy of the borophene structure itself, the phonon group velocities in $\vec{a}$ and $\vec{b}$ directions are different. The above analysis of Fig. 2(b) and Fig. 7 shows that (1) the influence of electric fields on the borophene structure is small; (2) the influence of the structural change on the thermal conductivity is negligible; and (3) the structural change is not reflected in the phonon spectrum. Therefore, in order to find out the root cause of the drastic increase and decrease in the thermal conductivity of borophene at electric fields of 0.04 V Å^{-1} and 0.4 V Å^{-1}, we need to explain from the perspective of phonon lifetime, which is another dominant factor of thermal conductivity.

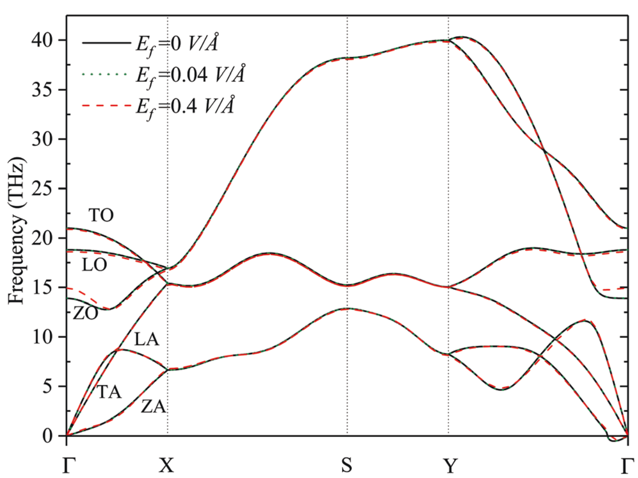

Fig. 7 Phonon dispersion of borophene under representative electric fields with phonon polarization labeled.

3.4 Phonon lifetime and anharmonicity

We present the frequency dependent phonon lifetime for some representative electric fields in Fig. 8. As shown in Fig. 8(a) and (b), the phonon lifetime at an electric field of 0.04 V Å^{-1} is obviously longer than that for the other two cases of electric fields, especially in the low frequency range of 7.5–10 THz. This variation trend of the lifetime is consistent with the lattice thermal conductivity of borophene with different electric fields, which means that phonon lifetime is the dominant factor for the dramatic change in lattice thermal conductivity as shown in Fig. 5(a). In addition, the unexpectedly low lattice thermal conductivity of borophene at a large electric field of 0.4 V Å^{-1} is mainly attributed to the suppressed phonon lifetime. The lifetime of borophene is generally below 100 ps, which is at least 4 orders of magnitude smaller than that of graphene's dominant ZA modes.[36,37] We further compared the lifetime of three acoustic branches at an electric field of 0.04 V Å^{-1} as shown in Fig. 8(b). The lifetimes of LA and TA branches are generally longer than that of ZA in the frequency range of 7.5–10 THz and the group velocities of LA and TA branches are also higher, so the LA and TA branches are the main contributors for lattice thermal conductivity of borophene. In fact, we found that with an electric field of 0.04 V Å^{-1}, the contribution of LA and TA branches to the overall thermal conductivity of borophene along $\vec{a}$ and $\vec{b}$ directions is 75.54% and 56.875%, respectively, which is obviously higher than that of the other acoustic branch and optical branches (below 30% for each).

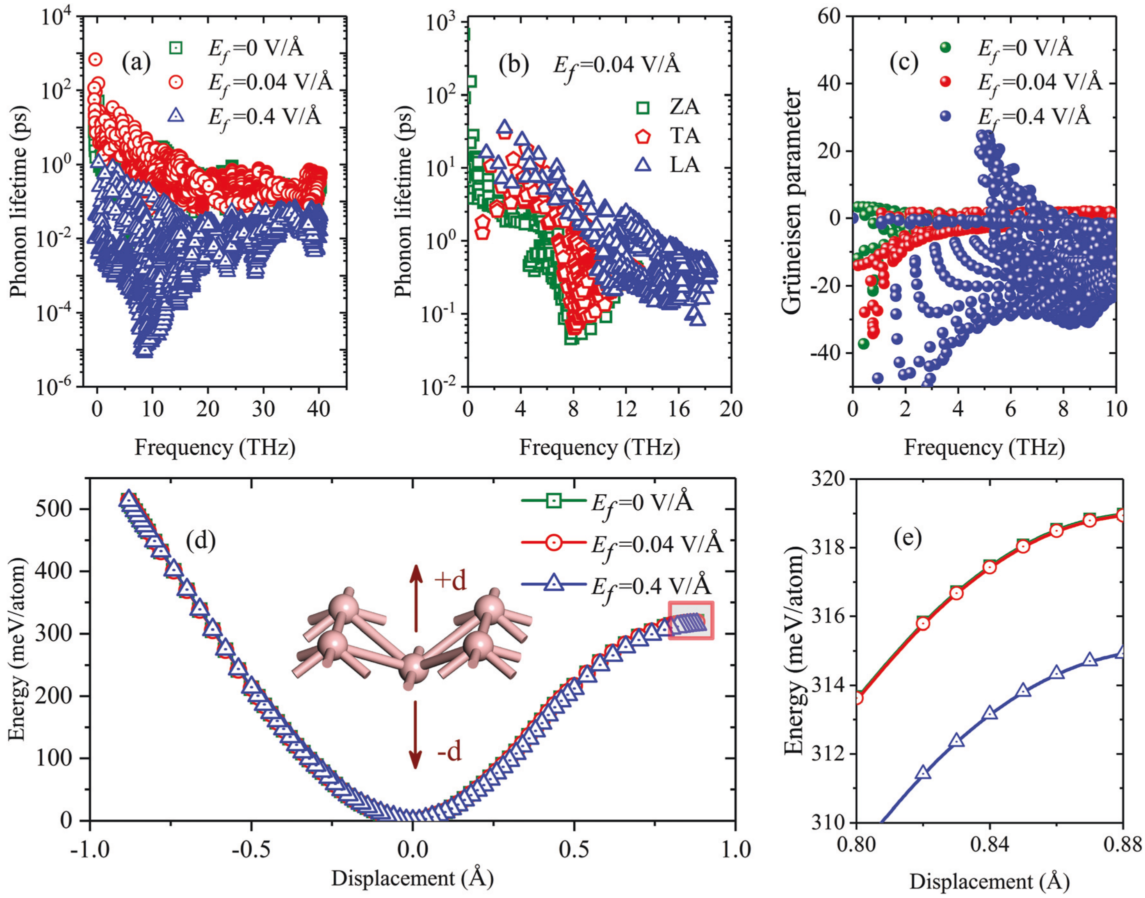

Fig. 8 (a) The phonon lifetime under representative electric fields. (b) Comparison of the phonon lifetime of three acoustic branches at an electric field of 0.04 V $Å^{-1}$. (c) The Grüneisen parameter of borophene under representative electric fields. (d) The potential energy change per atom with respect to the displacement of the boron atom along the out-of-plane direction. (e) Zoomed-in image of the potential energy change near the displacement of 0.80 Å.

For further insight into the anharmonic interactions, the scattering strength and the number of available phonon scattering channels are considered, which are characterized by the phase space[38] and the Grüneisen parameter.[39] Owing to the little differences in the phonon dispersion, the phase space of borophene changes slightly at different electric fields. The Grüneisen parameters are depicted in Fig. 8(c), and we found that the magnitude of the Grüneisen parameter is decreased greatly when an electric field of 0.4 V $Å^{-1}$ is applied. In contrast, the Grüneisen parameter at both electric fields (0 V $Å^{-1}$ and 0.04 V $Å^{-1}$) is higher apparently. Furthermore, the average Grüneisen parameters of borophene at electric fields of 0 V $Å^{-1}$, 0.04 V $Å^{-1}$, and 0.4 V $Å^{-1}$ are 0.476, 0.125, and −8.649, respectively. It is known that the larger the absolute value of the Grüneisen parameter, the stronger the anharmonicity. A lower absolute value of the Grüneisen parameter at an electric field of 0.04 V $Å^{-1}$ leads to higher thermal conductivity. Thus, the change in the phonon anharmonicity is the underlying mechanism for the variation of the phonon lifetime and further for the variation of the thermal conductivity of borophene upon applying an electric field.

The phonon anharmonic behavior can be traced back to the response of atomic and structure distortion. In order to have an intuitive understanding of the phonon anharmonicity, the potential well is depicted in Fig. 8(d). The potential well changes in a symmetric way when the boron atom vibrates around its equilibrium position along the $\vec{a}$ and $\vec{b}$ direction, while it changes in an asymmetric way for the out-of-plane directions [see Fig. 8(d)]. It is found that the potential well becomes flatter with stronger electric fields applied when boron oscillates along the out-of-plane direction, indicating more asymmetry and the nonlinear dependence of restoring forces on atomic displacement amplitudes.[40,41] In the meantime, the average Grüneisen parameters of the ZA branch at an electric field of 0 V $Å^{-1}$, 0.04 V $Å^{-1}$, and 0.4 V $Å^{-1}$ are calculated, and the results are −1.653, −4.041, and −27.737 respectively, which are consistent with the trend of the potential well under the electric field effect.

So far, the reason for the sudden increase in the anisotropy of borophene thermal conductivity at an electric field of 0.04 V $Å^{-1}$ has been identified. The intrinsic structure of borophene makes the phonon group velocity differ along the $\vec{a}$ and $\vec{b}$ direction, but this difference is relatively constant at different electric fields. According to eqn (1), the lattice thermal conductivity is the product of the three terms, namely specific heat capacity, group velocity, and phonon lifetime. Therefore, it is understandable that the phonon lifetime is an amplifying factor of the difference in the group velocity. Among all the representative electric fields, the phonon lifetime of borophene is enhanced obviously by applying an electric field of 0.04 V $Å^{-1}$. In particular, in the frequency region of 7.5–10 THz, the phonon lifetimes of LA and TA branches are significantly improved compared to that of the ZA branch, which amplifies the difference in the anisotropy of group velocity. Therefore, not only the thermal conductivity value itself increases steeply at an electric field of 0.04 V $Å^{-1}$, but also the anisotropy of the thermal conductivity is dramatically enhanced [see Fig. 6]. It is worth pointing out that, among all the methods for regulating the physical properties of materials, the external electric field acts relatively mildly, which not only has a negligible impact on the atomic structure of the material but also is reversible and thus the effect can go back and forth.

3.5 Insight from electronic structures

As mentioned above, the effect of the electric field on the value and anisotropy of borophene thermal conductivity is attributed to the phonon anharmonicity. Considering the inherent relationship between the phonon transport characteristics and the interatomic electrostatic interaction, we will explore the underlying mechanism responsible for the electric field regulated phonon transport characteristics and phonon anharmonicity from the perspective of electronic structures. The electron localization function (ELF) has already been used to characterize the interatomic bonding in lots of previous studies.[42–45] To understand the bonding characteristics in borophene, the ELF is calculated and the result is shown in Fig. 9. The ELF is a position dependent function with values that range from 0 to 1. ELF = 1 corresponds to perfect localization, ELF = 0.5 corresponds to the electron-gas like pair probability, and ELF = 0 corresponds to the electrons fully delocalized or electroless state. Fig. 9(a) shows the top view of the 3D ELF of borophene, where B_1 and B_2 are the upper and lower boron atoms, respectively. From Fig. 9(b) and (c), it is easily seen that the electrons are accumulated on the top of the upper plane and the bottom of the lower plane, indicating that the atomic orbitals of borophene contain more sp^3 hybridization. The sp^3 hybridization induces the buckled structure which stabilizes the whole crystal structure. Fig. 9(d) shows the ELF profile of borophene viewed along the (110) direction. The electronic charges are localized near B_1 and B_2 bonds, indicating strong covalent bonding between B_1 and B_2 atoms.

For an electric field of 0.4 V $Å^{-1}$ that significantly reduces the phonon lifetime and anisotropy, we explain it from the perspective of the electronic structure. The dielectric constant is a common physical concept in dielectric physics. It reflects the ability of charge in the material to be polarized at an applied electric field, thereby screening the external field, which is a crucial factor for carrier transport. Fig. 10(a) shows the dielectric constant of borophene with respect to the external electric field. With a small electric field applied (<0.02 V $Å^{-1}$), the charges are oriented in random direction, making the dielectric constant very slight. When the external electric field is bigger than 0.02 V $Å^{-1}$, it will polarize the charge by orienting the dipole moments, and the positive accumulation of charge and negative deletion of charges caused by the electric field lead to induced charges with opposite signs, which are located around the boron cores [see Fig. 10(c)]. The dielectric constant curve first increases until the external electric field reaches 0.04 V $Å^{-1}$, and then begins to decrease. By comparing the electric field-modulated thermal conductivity of borophene

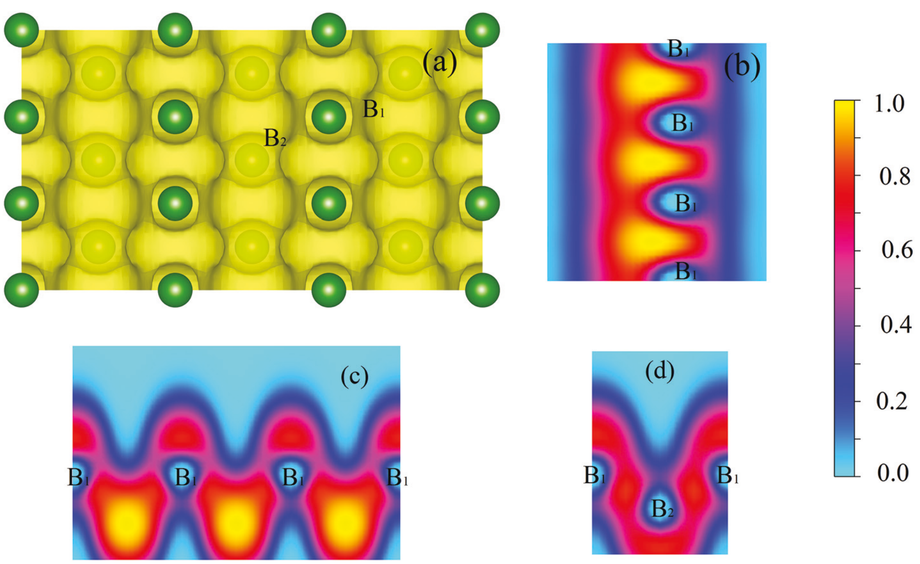

Fig. 9 The view of the 3D ELF and 2D electron localization function (ELF) profiles of borophene. (a) Top view (isosurface value = 0.6), side view along the (b) (100), (c) (010), and (d) (110) direction.

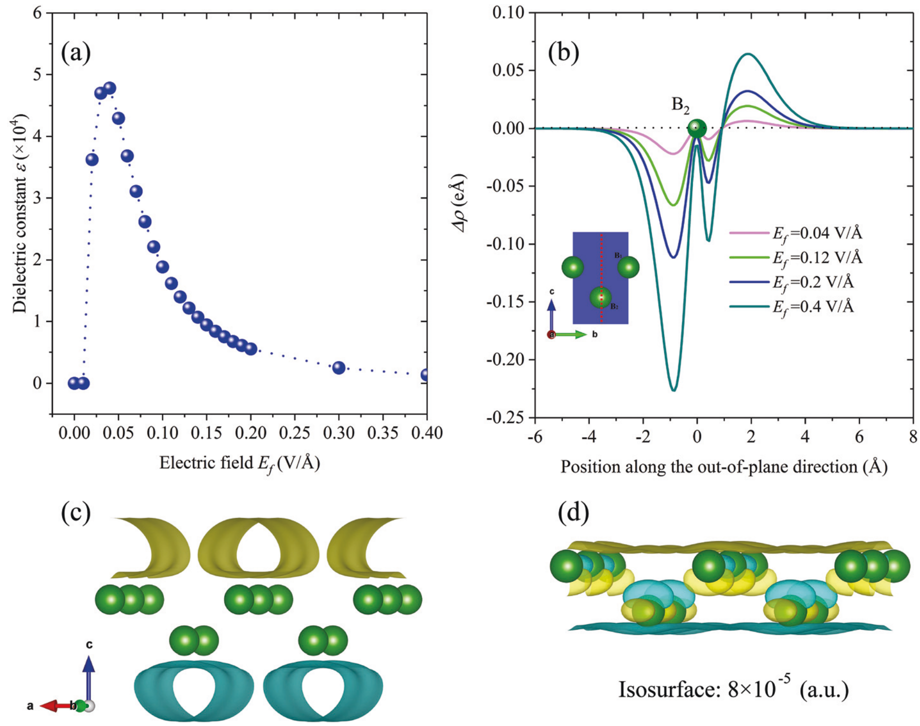

Fig. 10 (a) The dielectric constant as a function of the strength of external electric field. (b) The difference of charge density caused by the electric field ($\Delta\rho = \rho(E_f) - \rho(E_f = 0)$). Comparison of the difference of charge density distribution along the vertical path as shown in the inset (red dashed line). (c) The borophene difference of charge density at an electric field of 0.04 V Å^{-1}, the $\vec{a}$ and $\vec{b}$ directions are labeled (yellow: positive accumulation of charge, blue: negative depletion of charge). (d) The borophene difference of charge density at an electric field of 0.4 V Å^{-1}, the isosurface is set as 8×10^{-5} (a.u.).

[see Fig. 5(a)] with the dielectric constant, it is found that the variation trend of thermal conductivity is similar to that of the dielectric constant, which can be understood in terms of charge accumulation or depletion.[46] In order to study the effect of the electric field on the borophene charge environment, the charge density distribution without electric field is subtracted from the charge density distribution under each electric field. Fig. 10(b) shows the difference of charge density along the extracting path illustrated in the inset. It is found that the stronger the electric field, the more induced charges there are, and the screening effect will be stronger, therefore the dielectric constant will increase as the electric field increases (<0.04 V Å^{-1}). However, if the external electric field continues to increase (>0.04 V Å^{-1}), although more induced charges are generated, the induced charges are repelled away from the boron core by external electric field, and the dielectric constant decreases. This may be due to the fact that the ability of charge redistribution in the electric field is limited[46] or the polarizable charge is saturated.[47] Therefore, the charge environment between boron atoms is renormalized by the electric field which will lead to phonon renormalization and modulation of phonon anharmonicity.[48–51]

In addition, positive accumulation of charge appears in the negative range of boron atoms, and the negative depletion of charge should appear in the positive range of boron atoms, but more charge is accumulated in this range, because of the interaction between B_1 and B_2 atoms, which will affect the anisotropic character. Fig. 10(c) and (d) show the difference of charge density of borophene at an electric field 0.2 V Å^{-1} and 0.4 V Å^{-1}, respectively. It can be seen in Fig. 10(c) that the difference of electron density distribution is dense and continuous along the B_1–B_1 chain ($\vec{b}$ direction), while there are obvious gaps (discontinuous) between the chains along the $\vec{a}$ direction, which is the root cause of the anisotropy of thermal conductivity (group velocity in the $\vec{b}$ direction is higher than that in the $\vec{a}$ direction) [see Fig. 5(a)]. However, at an electric field of 0.4 V Å^{-1}, the difference of charge density exists along both $\vec{a}$ and $\vec{b}$ directions [see Fig. 10(d)], which reduces the anisotropy of thermal conductivity. Although it is challenging to quantitatively describe the behavior of the ELF and the difference of electric distribution, the above analysis evidently shows the variation of the charge environment experienced by the boron cores, which renormalizes the interactions between boron atoms and is believed to have a consequent influence on the phonon anharmonicity and further on the anisotropy of thermal conductivity.

4 Conclusions

In summary, first-principles calculations combined with phonon BTE are performed to systematically investigate the effect of external electric field on the thermal transport of monolayer borophene. At room temperature, the thermal conductivities of borophene first dramatically increase and then steeply decrease with the strength of electric field increasing. More interestingly, the intrinsic anisotropy of the thermal conductivity first increases to a peak value of 2.13 at an electric field of 0.04 V $Å^{-1}$. As the strength of electric field increases, the anisotropy of the thermal conductivity decreases and exhibits an oscillating behavior. The thermal transport in borophene finally transits into the isotropic regime when the strength of electric field is increased to 0.4 V $Å^{-1}$, *i.e.* the thermal conductivities in the two in-plane directions are almost equal despite the intrinsic anisotropic structure of borophene. The analysis of phonon related properties reveals that, due to the anisotropic structure, the difference in the phonon group velocity along $\vec{a}$ and $\vec{b}$ directions is the root cause of the intrinsic anisotropy of the thermal conductivity of borophene. With a moderate external electric field of 0.04 V $Å^{-1}$ applied, the phonon lifetime acts as an amplifying factor and thus the anisotropy of the thermal conductivity of borophene is substantially enlarged. At the highest strength of electric field of 0.4 V $Å^{-1}$, the phonon lifetime is extremely suppressed and eliminates the intrinsic difference in the phonon group velocity along $\vec{a}$ and $\vec{b}$ directions, resulting in isotropic thermal transport in borophene. The underlying mechanism is further understood in terms of the bonding characteristics and electron localization function. With an electric field applied, due to the screened potential resulting from the redistributed charge density, the interactions between boron atoms are renormalized, which leads to phonon renormalization and the modulation of phonon anharmonicity. Consequently, the thermal conductivity and anisotropy are drastically enhanced or reduced by the external electric field. The results obtained from this work unveil a general relationship between thermal transport and electric field for low-dimensional materials, and provide important guidance for designing nanomaterials with desirable thermal transport properties for specific energy applications.

Conflicts of interest

There are no conflicts to declare.

Acknowledgements

This project is supported by the PhD start-up fund of the Natural Science Foundation of Liaoning Province, China (Grant No. 20180540122, 200005636, and 200005720). Z. Y. gratefully acknowledges Dr Guangzhao Qin (Hunan University) and Dr Yufei Gao (Dalian University of Technology) for their helpful and fruitful discussions. K. Y. acknowledges the support from the China Scholarship Council. The research reported in this publication was supported in part by the NSF (award number 2030128) and SC EPSCoR/IDeA Program under NSF OIA-1655740 *via* SC EPSCoR/IDeA 20-SA05.

References

1 Z. A. Piazza, H.-S. Hu, W.-L. Li, Y.-F. Zhao, J. Li and L.-S. Wang, Planar hexagonal B36 as a potential basis for extended single-atom layer boron sheets, *Nat. Commun.*, 2014, **5**(1), 3113.

2 A. J. Mannix, X.-F. Zhou, B. Kiraly, J. D. Wood, D. Alducin, B. D. Myers, X. Liu, B. L. Fisher, U. Santiago, J. R. Guest, M. J. Yacaman, A. Ponce, A. R. Oganov, M. C. Hersam and N. P. Guisinger, Synthesis of borophenes: Anisotropic, two-dimensional boron polymorphs, *Science*, 2015, **350**(6267), 1513.

3 A. Lopez-Bezanilla and P. B. Littlewood, Electronic properties of 8−Pmmnborophene, *Phys. Rev. B*, 2016, **93**(24), 241405.

4 V. Wang and W. T. Geng, Lattice Defects and the Mechanical Anisotropy of Borophene, *J. Phys. Chem. C*, 2017, **121**(18), 10224–10232.

5 X. Liu, Z. Zhang, L. Wang, B. I. Yakobson and M. C. Hersam, Intermixing and periodic self-assembly of borophene line defects, *Nat. Mater.*, 2018, **17**(9), 783–788.

6 H. Cui, X. Zhang and D. Chen, Borophene: a promising adsorbent material with strong ability and capacity for SO2 adsorption, *Appl. Phys. A*, 2018, **124**(9), 636.

7 Z.-Q. Wang, T.-Y. Lü, H.-Q. Wang, Y. P. Feng and J.-C. Zheng, Review of borophene and its potential applications, *Front. Phys.*, 2019, **14**(3), 33403.

8 D. Li, Y. Chen, J. He, Q. Tang, C. Zhong and G. Ding, Review of thermal transport and electronic properties of borophene, *Chin. Phys. B*, 2018, **27**(3), 036303.

9 H. Zhou, Y. Cai, G. Zhang and Y.-W. Zhang, Superior lattice thermal conductance of single-layer borophene, *npj 2D Mater. Appl.*, 2017, **1**(1), 14.

10 B. Peng, H. Zhang, H. Shao, Y. Xu, R. Zhang and H. Zhu, The electronic, optical, and thermodynamic properties of borophene from first-principles calculations, *J. Mater. Chem. C*, 2016, **4**(16), 3592–3598.

11 B. Mortazavi, M.-Q. Le, T. Rabczuk and L. F. C. Pereira, Anomalous strain effect on the thermal conductivity of borophene: a reactive molecular dynamics study, *Phys. E*, 2017, **93**, 202–207.

12 Y. Liu, Y.-J. Dong, Z. Tang, X.-F. Wang, L. Wang, T. Hou, H. Lin and Y. Li, Stable and metallic borophene nanoribbons from first-principles calculations, *J. Mater. Chem. C*, 2016, **4**(26), 6380–6385.

13 H. Xiao, W. Cao, T. Ouyang, S. Guo, C. He and J. Zhong, Lattice thermal conductivity of borophene from first principle calculation, *Sci. Rep.*, 2017, **7**(1), 45986.

14 M. Gao, Q.-Z. Li, X.-W. Yan and J. Wang, Prediction of phonon-mediated superconductivity in borophene, *Phys. Rev. B*, 2017, **95**(2), 024505.

15 R. C. Xiao, D. F. Shao, W. J. Lu, H. Y. Lv, J. Y. Li and Y. P. Sun, Enhanced superconductivity by strain and carrier-doping in borophene: A first principles prediction, *Appl. Phys. Lett.*, 2016, **109**(12), 122604.

16 H. Wang, Q. Li, Y. Gao, F. Miao, X.-F. Zhou and X. G. Wan, Strain effects on borophene: ideal strength, negative Possion's ratio and phonon instability, *New J. Phys.*, 2016, **18**(7), 073016.

17 G. Kresse and J. Furthmüller, Efficiency of *ab initio* total energy calculations for metals and semiconductors using a plane-wave basis set, *Comput. Mater. Sci.*, 1996, **6**(1), 15–50.

18 G. Kresse and J. Furthmüller, Efficient iterative schemes for ab initio total-energy calculations using a plane-wave basis set, *Phys. Rev. B: Condens. Matter Mater. Phys.*, 1996, **54**(16), 11169–11186.

19 G. Kresse and D. Joubert, From ultrasoft pseudopotentials to the projector augmented-wave method, *Phys. Rev. B: Condens. Matter Mater. Phys.*, 1999, **59**(3), 1758–1775.

20 J. P. Perdew, K. Burke and M. Ernzerhof, Generalized Gradient Approximation Made Simple, *Phys. Rev. Lett.*, 1996, **77**(18), 3865–3868.

21 H. J. Monkhorst and J. D. Pack, Special points for Brillouin-zone integrations, *Phys. Rev. B: Solid State*, 1976, **13**(12), 5188–5192.

22 D. Huang and E. Kaxiras, Electric field tuning of band offsets in transition metal dichalcogenides, *Phys. Rev. B*, 2016, **94**(24), 241303.

23 W. Li, J. Carrete, N. A. Katcho and N. Mingo, ShengBTE: A solver of the Boltzmann transport equation for phonons, *Comput. Phys. Commun.*, 2014, **185**(6), 1747–1758.

24 A. Togo, F. Oba and I. Tanaka, First-principles calculations of the ferroelastic transition between rutile-type and CaCl2-type SiO2 at high pressures, *Phys. Rev. B: Condens. Matter Mater. Phys.*, 2008, **78**(13), 134106.

25 J. Yuan, L. W. Zhang and K. M. Liew, Effect of grafted amine groups on in-plane tensile properties and high temperature structural stability of borophene nanoribbons, *RSC Adv.*, 2015, **5**(91), 74399–74407.

26 G. Qin, Z. Qin, H. Wang and M. Hu, On the diversity in the thermal transport properties of graphene: A first-principles-benchmark study testing different exchange-correlation functionals, *Comput. Mater. Sci.*, 2018, **151**, 153–159.

27 S. Lee, K. Esfarjani, T. Luo, J. Zhou, Z. Tian and G. Chen, Resonant bonding leads to low lattice thermal conductivity, *Nat. Commun.*, 2014, **5**(1), 3525.

28 H. Sun, Q. Li and X. Wan, First-Principles Study of Thermal Properties of Borophene, *Phys. Chem. Chem. Phys.*, 2016, **18**, 14927.

29 G. Qin, Z. Qin, W.-Z. Fang, L.-C. Zhang, S.-Y. Yue, Q.-B. Yan, M. Hu and G. Su, Diverse anisotropy of phonon transport in two-dimensional group IV–VI compounds: A comparative study, *Nanoscale*, 2016, **8**(21), 11306–11319.

30 G. Qin, Q.-B. Yan, Z. Qin, S. Yue, M. Hu and G. Su, Anisotropic Intrinsic Lattice Thermal Conductivity of Phosphorene from First Principles, *Phys. Chem. Chem. Phys.*, 2014, **17**, 4854–4858.

31 H. Xie, M. Hu and H. Bao, Thermal conductivity of silicene from first-principles, *Appl. Phys. Lett.*, 2014, **104**(13), 131906.

32 X. Gu and R. Yang, First-principles prediction of phononic thermal conductivity of silicene: A comparison with graphene, *J. Appl. Phys.*, 2015, **117**(2), 025102.

33 D. T. Morelli and J. P. Heremans, Thermal conductivity of germanium, silicon, and carbon nitrides, *Appl. Phys. Lett.*, 2002, **81**(27), 5126–5128.

34 A. Jain and A. J. H. McGaughey, Strongly anisotropic in-plane thermal transport in single-layer black phosphorene, *Sci. Rep.*, 2015, **5**, 8501–8501.

35 D. K. Efetov and P. Kim, Controlling Electron-Phonon Interactions in Graphene at Ultrahigh Carrier Densities, *Phys. Rev. Lett.*, 2010, **105**(25), 256805.

36 L. Lindsay, W. Li, J. Carrete, N. Mingo, D. A. Broido and T. L. Reinecke, Phonon thermal transport in strained and unstrained graphene from first principles, *Phys. Rev. B: Condens. Matter Mater. Phys.*, 2014, **89**(15), 155426.

37 Y. Kuang, L. Lindsay, S. Shi, X. Wang and B. Huang, Thermal conductivity of graphene mediated by strain and size, *Int. J. Heat Mass Transfer*, 2016, **101**, 772–778.

38 M. E. Manley, O. Hellman, N. Shulumba, A. F. May, P. J. Stonaha, J. W. Lynn, V. O. Garlea, A. Alatas, R. P. Hermann, J. D. Budai, H. Wang, B. C. Sales and A. J. Minnich, Intrinsic anharmonic localization in thermoelectric PbSe, *Nat. Commun.*, 2019, **10**(1), 1928.

39 S. Zhang, B. Xu, Y. Lin, C. Nan and W. Liu, First-principles study of the layered thermoelectric material TiNBr, *RSC Adv.*, 2019, **9**(23), 12886–12894.

40 L.-D. Zhao, C. Chang, G. Tan and M. G. Kanatzidis, SnSe: a remarkable new thermoelectric material, *Energy Environ. Sci.*, 2016, **9**(10), 3044–3060.

41 W. G. Zeier, A. Zevalkink, Z. M. Gibbs, G. Hautier, M. G. Kanatzidis and G. J. Snyder, Thinking Like a Chemist: Intuition in Thermoelectric Materials, *Angew. Chem., Int. Ed.*, 2016, **55**(24), 6826–6841.

42 T. Ouyang and M. Hu, Competing mechanism driving diverse pressure dependence of thermal conductivity of *X*Te (X=Hg, Cd, and Zn), *Phys. Rev. B: Condens. Matter Mater. Phys.*, 2015, **92**(23), 235204.

43 G. Qin, Z. Qin, H. Wang and M. Hu, ., Lone-pair electrons induced anomalous enhancement of thermal transport in strained planar two-dimensional materials, *Nano Energy*, 2018, **50**, 425–430.

44 G. Qin, X. Zhang, S.-Y. Yue, Z. Qin, H. Wang, Y. Han and M. Hu, Resonant bonding driven giant phonon anharmonicity and low thermal conductivity of phosphorene, *Phys. Rev. B*, 2016, **94**(16), 165445.

45 G. Qin, Z. Qin, H. Wang and M. Hu, Anomalously temperature-dependent thermal conductivity of monolayer GaN with large deviations from the traditional $1/T$ law, *Phys. Rev. B*, 2017, **95**(19), 195416.

46 G. Qin, Z. Qin, S. Yue, Q.-B. Yan and M. Hu, External electric field driving the ultra-low thermal conductivity of silicene, *Nanoscale*, 2017, **9**, 7227.

47 T. Furukawa, K. Nakajima, T. Koizumi and M. Date, Measurements of Nonlinear Dielectricity in Ferroelectric Polymers, *Jpn. J. Appl. Phys.*, 1987, **26**(Part 1, No. 7), 1039–1045.

48 B. Liao, B. Qiu, J. Zhou, S. Huberman, K. Esfarjani and G. Chen, Significant Reduction of Lattice Thermal

Conductivity by the Electron-Phonon Interaction in Silicon with High Carrier Concentrations: A First-Principles Study, *Phys. Rev. Lett.*, 2015, **114**(11), 115901.

49 J. Zhuang, X. Xu, Y. Du, K. Wu, L. Chen, W. Hao, J. Wang, W. K. Yeoh, X. Wang and S. X. Dou, Investigation of electron-phonon coupling in epitaxial silicene by in situ Raman spectroscopy, *Phys. Rev. B: Condens. Matter Mater. Phys.*, 2015, **91**(16), 161409.

50 P. Zhang, S. G. Louie and M. L. Cohen, Nonlocal Screening, Electron-Phonon Coupling, and, Phonon Renormalization in Metals, *Phys. Rev. Lett.*, 2005, **94**(22), 225502.

51 J.-A. Yan, R. Stein, D. M. Schaefer, X.-Q. Wang and M. Y. Chou, Electron-phonon coupling in two-dimensional silicene and germanene, *Phys. Rev. B: Condens. Matter Mater. Phys.*, 2013, **88**(12), 121403.

